

Catalytic and photocatalytic performance of mesoporous Cu_xO–TiO₂

S. López-Ayala, M.E. Rincón*

Centro de Investigación en Energía-Universidad Nacional Autónoma de México, Materiales Solares, Privada Xochicalco S/N, Col. Centro, Apartado Postal 34, Temixco 62580, MOR, Mexico

ARTICLE INFO

Article history:

Received 8 June 2010

Received in revised form 5 April 2011

Accepted 26 May 2011

Available online 13 June 2011

Keywords:

Mesoporous
Titanium oxide
Copper
AB1 dye

ABSTRACT

In this work the synthesis of mesoporous Cu_xO–TiO₂ xerogels and their application in the catalytic and photocatalytic degradation of azo dye acid black 1 (AB1) are presented. To study the effect of Cu precursor, copper (II) formate, copper (II) chloride, and copper (II) nitrate were incorporated into the titanium alkoxide solution at various Cu/Ti atomic ratios. XRD, TEM, and N₂-adsorption studies evidenced the crystallite size and textural properties dependency on Cu-precursor and Cu/Ti ratio. All catalysts were mesoporous and underwent pore enlargement with increasing Cu content. They showed first order kinetics for AB1 discoloration with the reaction rate constant *k* being in the range of 0.2–0.5 min⁻¹ in catalytic degradation (dark experiments), slightly improving under diffuse illumination, and clearly increasing under UV light in catalysts obtained from inorganic precursors with large Cu content. Under dark conditions, degradation proceeds through a Fenton like mechanism, while under illumination it benefits from interfacial charge transfer from TiO₂ to Cu (II). Both mechanisms require an intimate contact between Cu (II) and titania, which is favored in catalysts formed from inorganic Cu-precursors, in contrast to formate precursors that favored bulk CuO formation.

© 2011 Elsevier B.V. All rights reserved.

1. Introduction

Due to its commercial availability, suitable optical and electronic properties, chemical stability and nontoxicity, titanium dioxide (TiO₂) has been the most studied support in heterogeneous catalysis [1,2]. Catalytic activity depends strongly on catalysts dispersion and size, as well as on the properties of the support [1–3], stimulating the study of various sizes and shapes of TiO₂ in both catalytic and photocatalytic applications [4,5]. Among the possible TiO₂ nanostructures, three dimensional (3-D) mesoporous titania and hierarchical meso-macroporous systems provide a compromise between pores big enough to be accessible by solvated reactants, and small enough to provide a substantial increase in surface area [6].

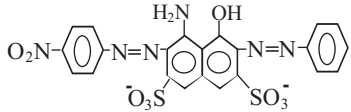
Among the various techniques to produce mesoporous materials, modified sol–gel methods are the most common to prepare mesoporous titania, either by introducing surfactant template molecules, ionic liquids, autoclaving at low temperature, or by subjecting the as-obtained xerogels to controlled calcination [1–3,6–11]. The combination of a large and accessible surface area with modifications caused by the presence of metal catalysts such as Ag, Cu, and Fe, have lead also to the improvement of TiO₂ visible light response and photocatalytic performance, depending of metal

content, nature of organic pollutant, and photoreaction medium [11–18]. Relevant mechanisms for maximizing TiO₂ photocatalytic activity include the generation of impurity energy levels in the band gap of TiO₂, preferential trapping of photogenerated carriers to avoid recombination of the e⁻/h⁺ pair, and formation of rectifying junctions between n-type TiO₂ and p-type semiconductors [13].

For Cu_xO–TiO₂ catalysts, numerous studies have shown improvement in the catalytic performance of titania supported CuO nanocatalysts [6,19–24], as well as in the photocatalytic activity of copper doped titania [11,16–18,25–27]. A synergistic catalytic interaction between copper oxide and TiO₂ was reported for CO oxidation [6,19,22], phenol oxidation [20], and NO reduction [21,23,24]. In these studies, the abundance of Cu⁺/Cu²⁺ and the dimension of CuO aggregates, correlated with the acidity of the support and with the catalyst activity for oxidation/reduction reactions. Additionally, with H₂O₂ present, homogeneous and heterogeneous Cu catalysts have shown the ability to produce non-selective, reactive OH radicals in a Fenton-like system [28,29], in close resemblance to oxidative photocatalysis. In regard to photocatalysis, photocatalytic activity of copper doped titania has been observed in photocatalytic reduction reactions and photocatalytic oxidative reactions. For photocatalytic reduction reactions such as conversion of CO₂ into small organic compounds, doping with Cu (II) was reported as very efficient, although the presence of Cu (I) played a significant role [16,25,26]. For photocatalytic oxidation of organic molecules, mineralization was found to depend on Cu

* Corresponding author. Tel.: +52 555 6229742; fax: +52 555 6229752.
E-mail address: merg@cie.unam.mx (M.E. Rincón).

Table 1
Chemical characteristics of acid black 1 (AB1).

Acid black 1	Synonymous: 8-amino-7-(p-nitrophenylazo)-2-phenylazo disodium salt, Naphthol blue black (Aldrich)	
C.I. No.	20470	Chemical structure
		
Formula	C ₂₂ H ₁₄ N ₆ Na ₂ O ₉ S ₂	
λ _{max} (nm)	618	
Dye content (%)	50	
Color	Black blue	

content [20,30,31], and on the formation of stable Cu (I) [20]. Note that we use the label Cu_xO–TiO₂ as a generic label for both catalysts and photocatalysts, and the term *copper doped titania* when the semiconducting properties of TiO₂ or its photoreactivity have been shown to be affected by Cu content. Most Cu_xO–TiO₂ catalysts/photocatalysts have been obtained as fine precipitates, using impregnation and co-precipitation methods [30–33] and alkoxide sol–gel process [34], leaving the issue of easy recovery aside.

Abundance of Cu²⁺/Cu⁺ species in Cu_xO–TiO₂ depends on the synthesis conditions, as the nature, size, and stability of numerous catalyst active phases are affected by the interactions between the different anions and the embryonic titania particles [35–37]. Moreover, Cu content determines the catalytic and photocatalytic performance, but no works were found in the literature where both contributions were studied with the same model reaction. Here, we report a systematic study with various Cu-precursors and Cu/Ti contents, to study the effect on texture, surface composition, and surface structure of mesoporous Cu_xO–TiO₂, and to assess the synthesis conditions leading to doping (Cu-doped TiO₂) or to titania supported CuO nanocatalysts. The catalytic and photocatalytic performance of these species were validated in the degradation of acid black 1 (AB1); for practical reasons, degradation took place under dark conditions, standard laboratory light, and UV-light. Table 1 shows the main characteristic of the selected azo dye, a pollutant of high environmental impact [38,39]. This dye was mineralized in minutes by mesoporous granules that were easily separated from the solution by decantation, and advantage over smaller particles obtained by depositing Cu ions by wet impregnation on commercial TiO₂ (Degussa P25) or sol–gel processed TiO₂.

2. Experimental

2.1. Synthesis and characterization

Copper containing titania gels were obtained by the sol–gel method using titanium tetra-isopropoxide (Aldrich), high purity water (Millipore Milli-Q water, 18.2 MΩ), ethanol (JT Baker), HCl (Merck), and by adding various copper (II) salts (Aldrich: formate, chloride; Riedel de Haën: nitrate). The molar ratio of the components in the sol–gel bath was adjusted to H₂O/Ti = 4.8, EtOH/Ti = 45, and H⁺/Ti = 0.23. After gelation at room temperature for one day, the monolithic gels were subjected to the following heating program in air: 2 h at 90 °C, 1 h at 150 °C, and 1 h at 450 °C, adjusting the heating rate to 10 °C/10 min. The calcined gel was obtained in the form of small granules, characterized according to standard sieving tests (NOM-C-329-191-4). The apparent density of the calcined xerogels was calculated by weighting a specific amount of material and measuring its volume in a 10 mL graduated cylinder.

Materials characterization was carried out by different techniques such as X-ray diffraction (Rigaku Dmax 2200 diffractometer, with CuK_α radiation (λ = 1.5405 Å)), thermogravimetric analyses (TG, 2960 Universal TA Instruments, scanned at 10 °C/min under

nitrogen gas), transmission electron microscopy (JEOL JEM-2100F), and nitrogen adsorption isotherms (surface area and micropore size analyzer NOVA 1200e) modelled by the non local density functional theory (NLDFT) for surface area determination, and by the Barrett–Joiner–Halenda (BJH) model for pore size-volume distribution. Band gap values were calculated from diffuse reflectance spectra obtained in a Shimadzu UV-31001PC spectrometer equipped with an integration sphere, using a thick layer of granules as sample and barium sulphate as reference. The Kubelka–Munk function was used to transform the diffuse reflectance spectra into a magnitude proportional to the extinction coefficient (α), using the equation:

$$F(R) = \frac{\alpha}{s} = \frac{(1 - R)^2}{2R}$$

where *s* is the scattering coefficient assumed constant in the energy range considered. The extinction coefficient was corrected by sample porosity (*p*) using the equation:

$$\alpha_c = \frac{\alpha}{1 - p}$$

Porosity was determined from the ratio of pore volume (obtained from nitrogen isotherms) and total volume (i.e., pore volume plus titania volume computed from a density of 4.2 g/cm³).

2.2. Degradation of acid black 1

Acid black 1 solution was prepared by dissolving acid black 1 powder in distilled water to obtain a 100 mg/L concentration. The absorbance of this solution was close to 1 after diluting by a factor of 5. The degradation experiments were carried at pH 3 in a 250 mL beaker containing 100 mL of acidified AB1 solution, a variable amount of H₂O₂, and 0.5 g/L of Cu_xO–TiO₂ calcined gel. A sample port, a thermometer, and a long pipette were used to monitor the reaction conditions and to keep the volume constant (i.e., to condense any volatile organic intermediates formed during AB1 decomposition). Degradation experiments were performed at various temperatures, H₂O₂ dosage in the range of 0.5–3.4 g/L, and with catalysts synthesized at three Cu/Ti atomic ratios with organic and inorganic Cu-precursors. Degussa TiO₂ P25 was used to assess the performance of the calcined TiO₂ and Cu_xO–TiO₂ xerogels. For dark experiments, pyrex flasks painted black were used as black containers, while for experiments carried out at standard laboratory illumination, the container was transparent and the illumination intensity in the range of 0.4 W/m². For UV-experiments, a black light UV-lamp with 4.05 W/m² illumination intensity was immersed in the 250 mL flask. Dye degradation/discoloration was followed by monitoring the absorbance at 618 nm wavelength and by determining the total organic carbon and color disappearance in units of Pt–Co (Hach colorimeter, DR/800).

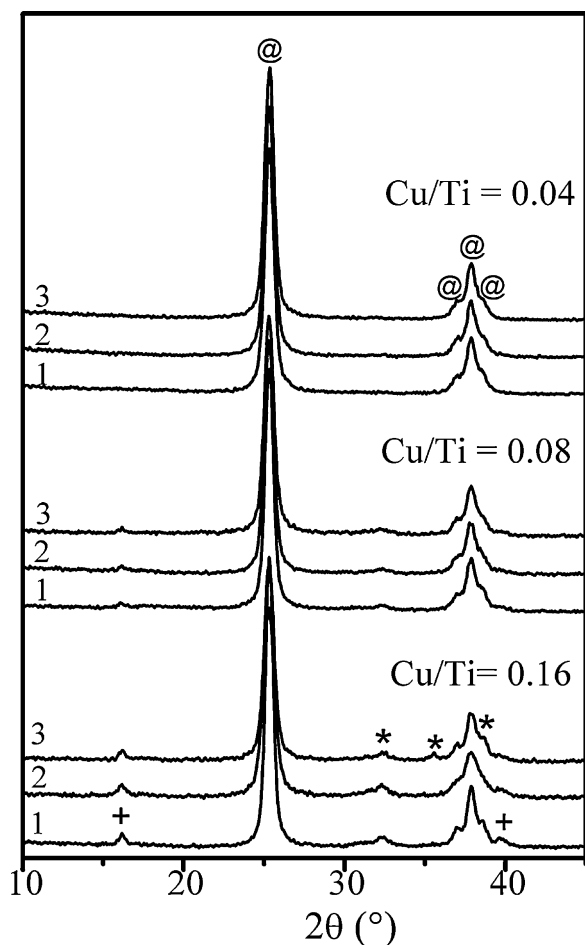


Fig. 1. XRD patterns of $\text{Cu}_x\text{O-TiO}_2$ catalysts synthesized with various Cu/Ti ratios and Cu (II) salts: (1) $\text{Cu}(\text{HCO}_2)_2$, (2) $\text{Cu}(\text{NO}_3)_2$, (3) CuCl_2 . Anatase/@; $\text{Cu}(\text{OH})_2$ /*; CuO /+.

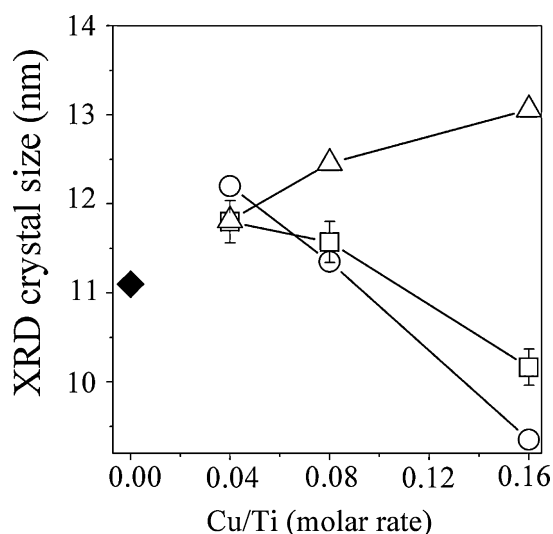


Fig. 2. Crystal size obtained from the anatase (101) reflection of $\text{Cu}_x\text{O-TiO}_2$ samples synthesized at various Cu/Ti ratios and Cu (II) salts: (Δ) $\text{Cu}(\text{HCO}_2)_2$, (\circ) $\text{Cu}(\text{NO}_3)_2$, (\square) CuCl_2 . Cu-free TiO_2 (\blacklozenge).

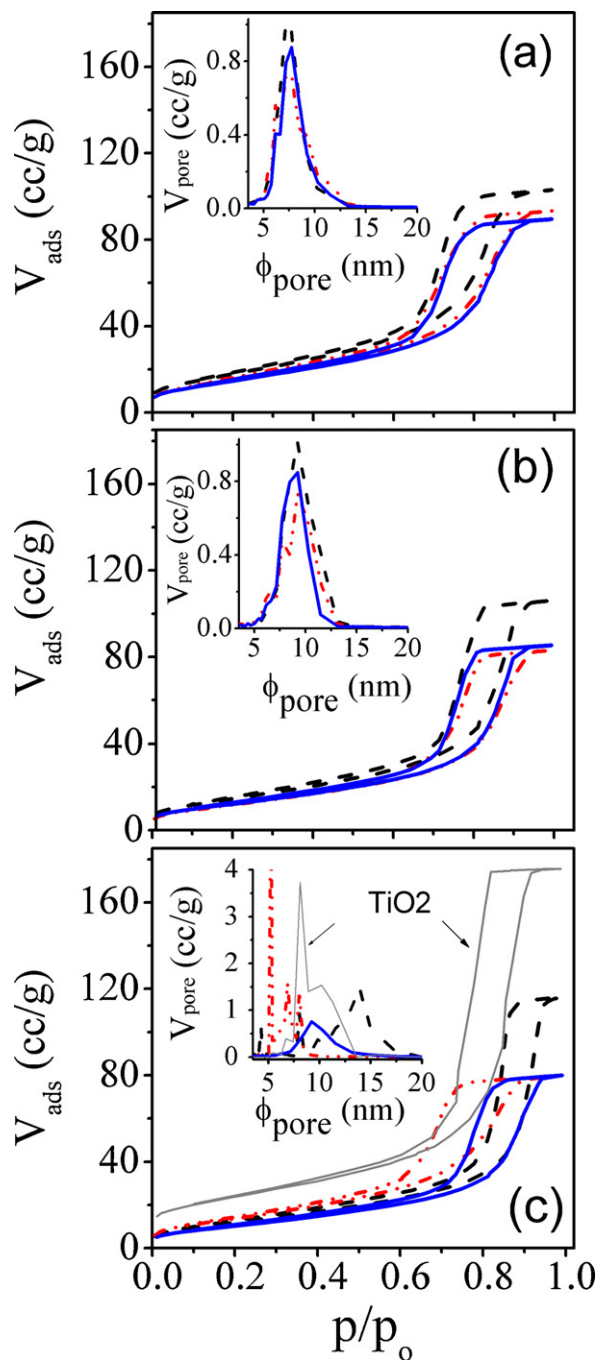


Fig. 3. N_2 adsorption-desorption isotherms and pore size distribution (inset) of calcined xerogels. Cu/Ti = 0.04 (a), 0.08 (b), 0.16 (c). Cu (II) salt: (---) $\text{Cu}(\text{HCO}_2)_2$, (-·-·-·) $\text{Cu}(\text{NO}_3)_2$, (-) CuCl_2 .

3. Results

3.1. $\text{Cu}_x\text{O-TiO}_2$ characterization

Under co precipitation reactions, Cu (II) can be chemically attached to the TiO_2 surface through oxygen atoms and be incorporated in a distorted CuO -like structure, or well, occupied interstitial/substitutional positions in the titania network [16,17,40–42]. Fig. 1 shows the X-ray diffraction patterns of calcined xerogels as a function of Cu/Ti ratio and Cu salts, where it is evident that crystallization is affected by Cu content. For Cu/Ti = 0.04, just anatase peaks (JCPDS 21-1272) are apparent, while at higher Cu/Ti ratios the X-ray diffraction patterns show addi-

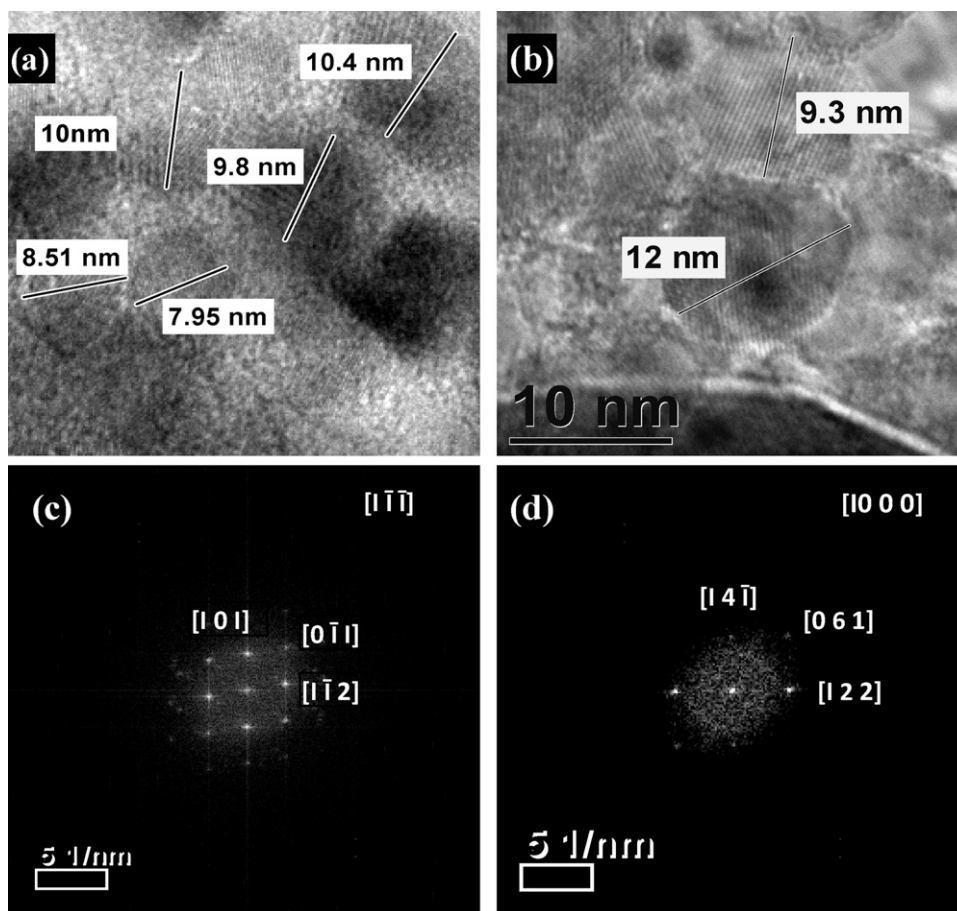


Fig. 4. TEM images of TiO_2 (a) and $\text{Cu}_x\text{O-TiO}_2$ (b–d), showing the crystalline patterns of anatase (c) and $\text{Cu}(\text{OH})_2$ (d).

tional peaks assigned to CuO (JCPDS 45-0937) and $\text{Cu}(\text{OH})_2$ (JCPDS 13-0420). At the lowest Cu/Ti ratio, magnification of the anatase (101) reflection does evidence a small shift in comparison with the copper-free sample. Interstitial incorporation of Cu into the titania network seem to be taken place at this ratio, while segregation and growth of Cu compounds at the titania surface occur at higher Cu content, affecting further nucleation and growth of titania particles, as seen in the distinct trends of anatase crystallite size vs. Cu/Ti ratio shown in Fig. 2. In this figure, an increment in crystallite size with Cu content is clear in materials based on Cu-formate, in contrast with the crystal reduction of those based on inorganic Cu-precursors, which at Cu/Ti = 0.16 are even smaller than the Cu-free titania. The values of crystal size were calculated from the Debye–Scherrer equation, using the anatase (101) reflection. We notice that crystallite size also influences the fracture of xerogels during annealing, giving similar tendencies of granule size vs. Cu/Ti ratio. Granules originated from Cu-formate increase in size at higher Cu content and have equivalent diameters in the range of 0.7–1.5 mm, while Cu-nitrate and chloride produce smaller granules in the range of 0.5–1 mm, and show a decrement in size with increasing Cu content. At all Cu/Ti ratios the calcined xerogels had the black coloration typical of Cu (II). Apparent density (AD) determinations (Table 2) evidenced the lower compactation of calcined $\text{Cu}_x\text{O-TiO}_2$ xerogels synthesized with Cu-formate, and the increase in AD as the Cu/Ti ratio increases.

Catalysts mesoporosity was verified by N_2 adsorption-desorption isotherms. For all Cu/Ti ratios, and with all Cu-precursors, a hysteresis loop indicative of mesoporosity is noticeable in Fig. 3. Estimation of surface area and pore diameter

by the non-linear density functional model (S_{NLDFT}) and the BJH model (D_{pBJH}), indicate strong similarities in pore size distribution (~7–9 nm) at the lowest Cu/Ti ratios for all Cu-precursors. Fig. 3(a and b) depict this resemblance, as well as the increase in pore size as the Cu/Ti ratio increases. Pore volume at the peak of the distribution follows the order $\text{Cu}(\text{HCO}_2)_2 > \text{CuCl}_2 > \text{Cu}(\text{NO}_3)_2$. At Cu/Ti = 0.16, each Cu-precursor has a distinct pore size distribution, with the one corresponding to Cu-formate shifted to larger pore values (maximum at 14 nm), and the one corresponding to Cu-nitrate to lower values (several maximums between 4 and 10 nm). The calcined Cu-free TiO_2 xerogel shows the largest adsorption volumes (~170 cc/g), and a bimodal distribution of pores peaking at 7.5 and 10 nm. Table 2 summarizes the S_{NLDFT} values and from them it is evident that they go down with the increase in Cu/Ti ratio due to the enlargement in pore diameter. For all Cu-doped materials, S_{NLDFT} is in the range of 32–51 m^2/g , while TiO_2 P25 has $S_{\text{NLDFT}} = 48 \text{ m}^2/\text{g}$. It is noteworthy to say that we grinded the

Table 2
Textural properties of $\text{Cu}_x\text{O-TiO}_2$ catalysts.

Copper salt	Cu/Ti (mol/mol)	AD (mg/mL)	S_{NLDFT} (m^2/g)	D_{pBJH} (nm)
$\text{Cu}(\text{HCO}_2)_2$	0.04	1.02	51	7
	0.08	1.10	44	9
	0.16	1.17	38	16
$\text{Cu}(\text{NO}_3)_2$	0.04	1.06	45	7
	0.08	1.16	36	9
	0.16	1.22	42	4
CuCl_2	0.04	1.08	43	8
	0.08	1.13	37	9
	0.16	1.18	32	9

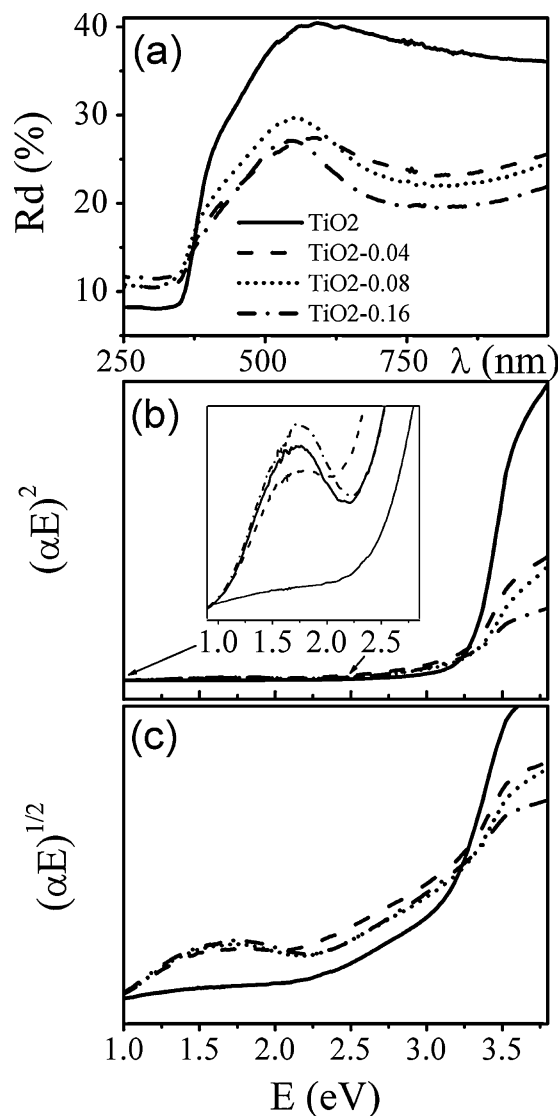


Fig. 5. Optical properties of $\text{Cu}_x\text{O-TiO}_2$ obtained from Cu-chloride precursors: (a) diffuse reflectance (R_D) spectra, (b) direct optical transitions, (c) indirect optical transitions.

granules and found similar values, confirming that the surface area and pore volume corresponds primarily to the interior of each granule. Hence, the granule size does not compromise the catalytic or photocatalytic activity, just facilitates the recovery of the materials.

To better understand the interaction of Cu and Ti precursors, the size of CuO and Cu(OH)_2 clusters were analyzed by TEM in catalysts synthesized at $\text{Cu/Ti}=0.16$. At this Cu content, XRD data suggests the formation of coupled CuO/TiO_2 composites, instead of the incorporation of Cu into the titania network. Fig. 4 corresponds to TEM images of pulverized TiO_2 [Fig. 4(a)] and $\text{Cu}_x\text{O-TiO}_2$ obtained from CuCl_2 precursors [Fig. 4(b)]. The polydispersity of Cu containing clusters ranges from 2.5 nm to 10 nm, and mask differences due to Cu-precursor and/or Cu-content. HRTEM images followed by FFT analysis confirm the presence of anatase [Fig. 4(c)] and Cu(OH)_2 [Fig. 4(d)], while the absence of well formed crystalline planes made the identification of CuO more difficult.

Catalysts photoactivity was assessed from their reflectance spectra and band gap estimation assuming direct and indirect optical transitions. As can be seen in Figs. 5 and 6, catalysts obtained from Cu-chloride (Fig. 5) and Cu-formate (Fig. 6) show a strong

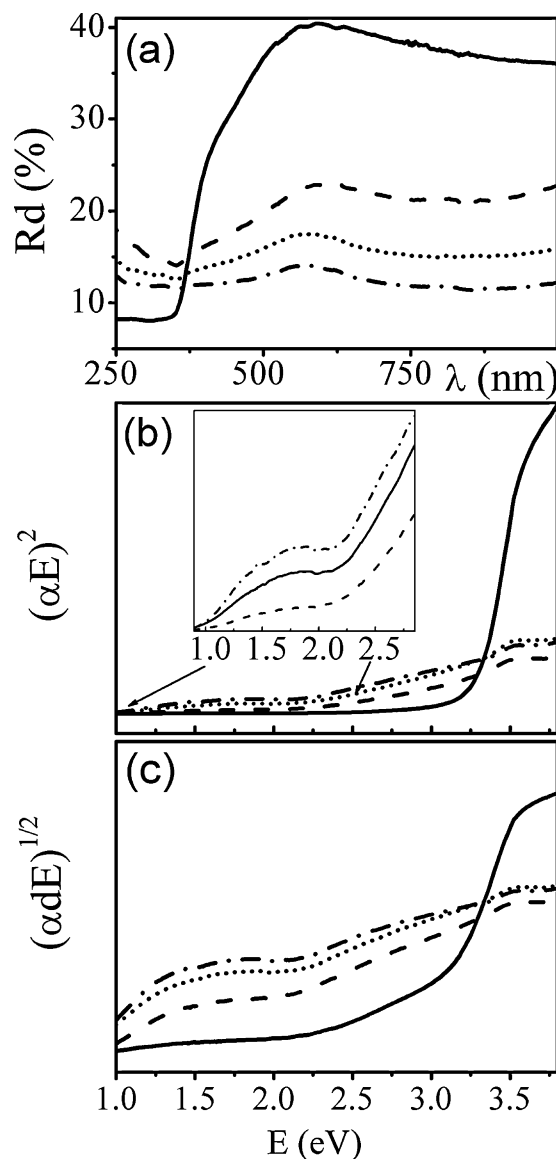


Fig. 6. Optical properties of $\text{Cu}_x\text{O-TiO}_2$ obtained from Cu-formate precursors: (a) diffuse reflectance (R_D) spectra, (b) direct optical transition, (c) indirect optical transitions.

effect on Cu/Ti ratio, with titania's E_g shifting to the red as the amount of Cu increases, the narrowing of the band gap is in the range of the one reported recently by López et al. [17]. In addition to the band-band absorption, a Cu-dependent absorption near 1.5 eV and a shoulder at 2.75 eV are also evident. The first is related to $2E_g \rightarrow 2T_g$ transitions of Cu^{2+} [16,17], and the last to the direct interfacial charge transfer (IFCT) from the valence band of TiO_2 to Cu (II) (i.e., to the presence of Cu (I) clusters reduced from CuO clusters) [16,17], or to the band gap of bulk p-type CuO [43,50]. Since the 2.75 eV shoulder becomes more notorious in the optical transitions of catalysts produced with Cu-formate, it lead us to think that organic copper precursors favor the formation of CuO instead of the introduction of Cu into the titania network.

3.2. Degradation of AB1 with $\text{Cu}_x\text{O-TiO}_2$

Degradation of AB1 was studied as a function of temperature and H_2O_2 dosage, in addition to the parameters differentiating the here considered catalysts. Degradation proceeded at fixed $\text{pH}=3$, with 0.5 g/L catalyst, and 100 mg/L AB1 (C_0). Previous to these

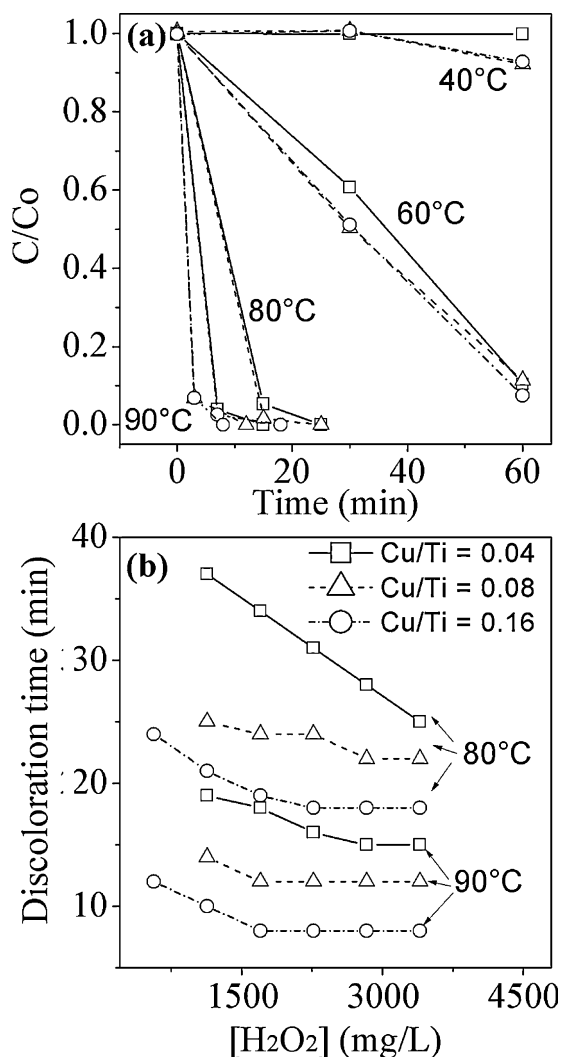


Fig. 7. AB1 discoloration achieved at pH 3 by 0.5 g/L Cu_xO-TiO_2 catalysts synthesized with $CuCl_2$ as the Cu precursor: (a) effect of temperature, $[H_2O_2] = 3.4$ mg/L, (b) effect of H_2O_2 dosage. Cu/Ti ratios indicated in (b) are also valid for (a). Experiments performed under laboratory diffuse light ($0.4 W/m^2$).

experiments, adsorption experiments were carried out at room temperature for 24 h, finding 3% adsorption in Cu-free catalysts (i.e., 3 mg dye/0.5 g catalyst). For Cu-doped titania, dye degradation was obvious at room temperature after 24 h, therefore in these catalyst adsorption of products was pursued, placing the catalysts in ethanol and measuring the color obtained, none of the Cu-doped catalysts shows any color. Fig. 7(a and b) shows the effect of temperature and H_2O_2 dosage in AB1 discoloration using Cu_xO-TiO_2 catalyst synthesized with $CuCl_2$ at various Cu/Ti ratios. The decay of C/C_0 vs. time is not related to dye removal by adsorption processes, given that at 40 °C C/C_0 remains close to unity beyond 60 min [see Fig. 7(a)]. Dye adsorption was observed at room temperature in the Cu-free catalysts but was not obvious in Cu-doped titania due to its color; above 40 °C, adsorption was not observed in any of the catalysts. As seen in Fig. 7, degradation depends strongly on temperature, and proceeds in few minutes at $T > 80$ °C. The quickest degradation corresponds to the highest Cu/Ti ratio and the highest T . Fig. 7(b) shows plots of discoloration time vs. H_2O_2 at 80 °C and 90 °C, where at 2 g/L H_2O_2 most catalysts reach a plateau and further H_2O_2 dosage does not improve the reaction time.

Degradation under dark, diffuse laboratory light, and UV illumination are shown in Figs. 8 and 9, as a function of Cu-precursor, at the highest and lowest Cu/Ti ratio, respectively. Degradation

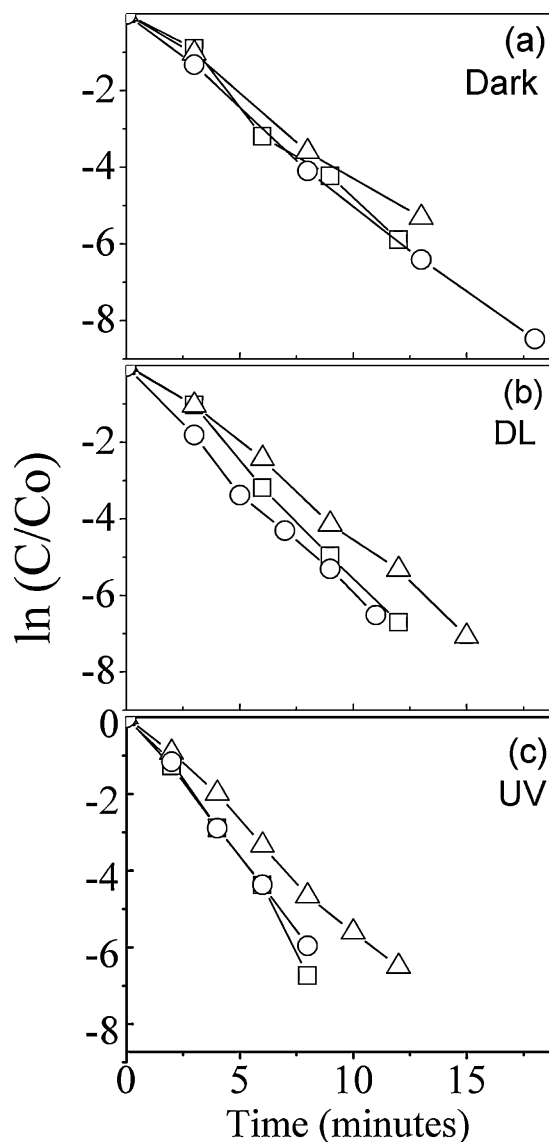


Fig. 8. First order kinetics for AB1 degradation at 80 °C, pH 3, 3.4 mg/L H_2O_2 , and 0.5 g/L catalyst. Catalysts were obtained at Cu/Ti=0.16, with Cu-formate (Δ), Cu-chloride (\square), and Cu-nitrate (\circ). (a) Experiments under dark; (b) experiments under laboratory diffuse light ($0.4 W/m^2$); (c) experiments with black UV lamps ($4 W/m^2$).

took place at 80 °C, pH 3, with 3.4 mg/L H_2O_2 , and 0.5 g/L catalyst. A linear relationship between $\ln(C/C_0)$ and time is obtained at all Cu/Ti ratios, validating the assumption of first order reaction. Comparable decay curves originate from catalysts synthesized from $CuCl_2$ and $Cu(NO_3)_2$ salts, but catalysts from formate precursor show consistently the slowest decay curve, and the difference magnifies at lower Cu/Ti ratios and under illumination (i.e., at the synthesis conditions leading to doping). For Cu/Ti=0.16, discoloration times follow the order $t_{UV} (\sim 12 \text{ min}) < t_{DL} (\sim 15 \text{ min}) < t_{Dark} (\sim 20 \text{ min})$. The reaction rate constant k for all precursors, Cu/Ti ratios, and illumination regime are illustrated in Fig. 10. k is in the range of 0.2–0.5 min^{-1} in catalytic processes taking place under dark; minor improvement occurs under diffuse illumination, with k in the range of 0.2–0.6 min^{-1} , whereas under UV illumination the improvement is more clear, as TiO_2 and CuO photoactivation might open up photocatalytic routes, given k in the range of 0.2–0.8 min^{-1} . Notice that the increase in photoreactivity is more obvious at larger Cu content and with the inorganic Cu-precursors. Catalytic/photocatalytic reactivity follow the order: $CuCl_2 \approx Cu(NO_3)_2 > Cu(HCO_2)_2$. For Cu-free titania the

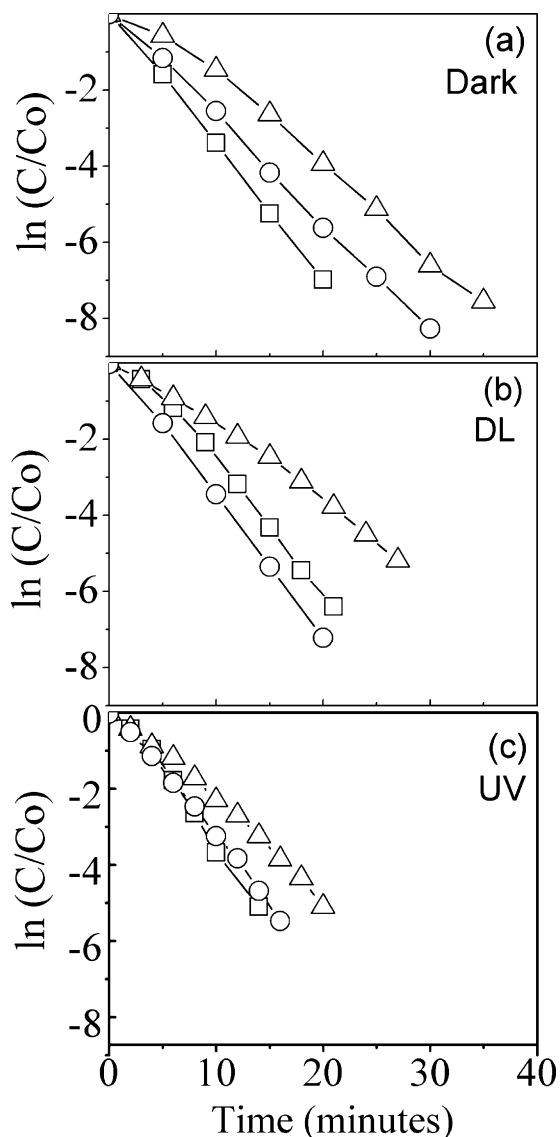


Fig. 9. First order kinetics for AB1 degradation at 80 °C, pH 3, 3.4 mg/L H₂O₂, and 0.5 g/L catalyst. Catalysts were obtained at Cu/Ti=0.04, with Cu-formate (Δ), Cu-chloride (\square), and Cu-nitrate (\circ). (a) Experiments under dark; (b) experiments under laboratory diffuse light (0.4 W/m²); (c) experiments with black UV lamps (4 W/m²).

value of k was negligible under dark and diffuse illumination, and one order of magnitude lower under UV illumination $k_{UV} [\text{TiO}_2 = 0.025 \text{ min}^{-1}]$.

Looking to the values of k in terms of each specific precursor, the catalytic and photocatalytic reactivity of formate based materials enhances by 100% as the Cu/Ti ratio goes from 0.04 to 0.16. For nitrate and chloride based catalysts, the increase in catalytic activity is around 50% (nitrate) and 40% (chloride) as the Cu/Ti ratio increases, while the enhancement on photoreactivity is in the range of 80% (nitrate) to 100% (chloride). Apparently, the amount and semiconducting properties of CuO can account for the enhancement in catalytic and photocatalytic reactivity in formate based catalysts, but for the inorganic precursors doping of titania seems more important. Trying to correlate catalysts performance with their textural properties, relative to formate, inorganic precursors lead to materials with smaller crystal size (titania), reduced pore diameter, and inferior S_{NLDFT} . Therefore, their superior performance might be due to the lack of bulky CuO on the titania matrix, and/or the abundance of nanodispersed CuO

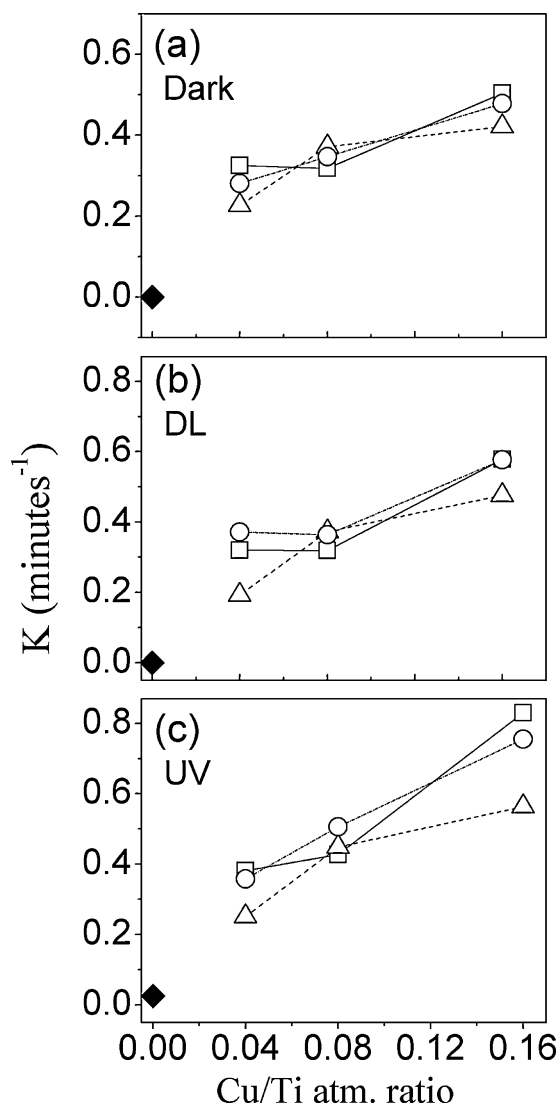


Fig. 10. AB1 discoloration rate constant k as a function of Cu/Ti ratio for the various Cu_xO-TiO₂ catalysts. [AB1] = 100 mg/L, $T = 80$ °C, pH = 3, [catalyst] = 0.5 g/L. Cu (II) salt: (Δ) Cu(HCO₂)₂, (\circ) Cu(NO₃)₂, (\square) CuCl₂. Cu-free TiO₂ (Δ).

combined with the more likely insertion of Cu into the titania matrix.

The granules retrieval from wastewater and reuse were also tested at various pH. Most catalysts were reused with good reproducibility for up to 6 degradation experiments without attempting reactivation and/or filtration. For those containing the highest Cu/Ti ratio, dissolution of copper was around 0.2% with respect to the original Cu content, changing very little from the first cycle (0.24%) to the last cycle (0.20%). For catalysts with fine grains such as those obtained with Cu-chlorides, mass lost accounts for 30% at the 6th cycle. The effect of pH in reaction time, Pt-Co color, and lixiviation of Cu are shown in Fig. 11 for Cu-chloride catalysts (the best materials) performing at 90 °C. Low pH favors lower reaction times but also more Cu-free, although this is well below the maximum limit. Maximum contaminant level goal for Cu-free is 1.3 mg/L for drinking water [44].

To further corroborate the amount of mineralization obtained at lower H₂O₂ dosage and with intermediate Cu/Ti ratio of 0.08, parallel experiments were carried out at 80 °C and [H₂O₂] = 1.7 mg/L with the Cu-chloride catalyst. The determination of TOC and color in Pt-Co units was compared with those of commercial TiO₂ (P25-Degussa) and Cu-free TiO₂ granules. Under normal lab illumination,

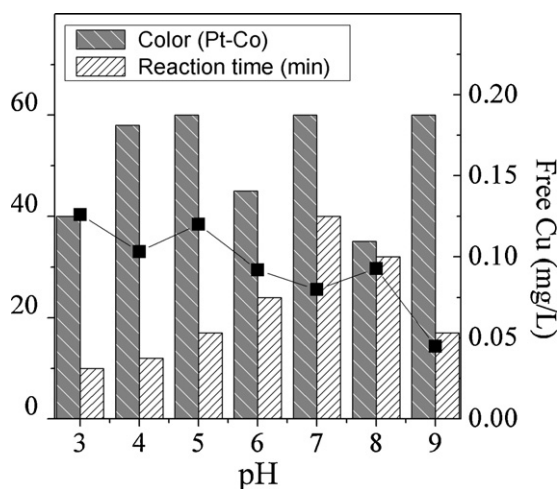


Fig. 11. Effect of pH in reaction time, Pt–Co color, and Cu lixiviation from Cu–chloride catalysts. [AB1] = 100 mg/L, $T = 90^\circ\text{C}$, [catalyst] = 0.5 g/L. Experiments under laboratory diffuse light (0.4 W/m^2).

the latest did not show any discoloration in the 24 min interval tested, in clear contrast to the changes observed in the absorbance spectra of dyes discolored by $\text{Cu}_x\text{O-TiO}_2$ granules, where the values of TOC and color (Table 3) indicated 58–72% mineralization.

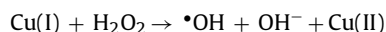
4. Discussion

Discoloration of aqua solutions of AB1 (50 mg/L) by photooxidation ($\text{UV}/\text{H}_2\text{O}_2$) has been reported by Shu and Chang [45,46]. They used relatively high volumetric radiation dosage (i.e., 750–5000 W/L), obtaining complete discoloration in 7 min, as well as first order kinetics. Lower radiation dosage (8 W UV lamp) and bimetallic Cu–Fe catalysts were used by Yip et al. [47] in the photodegradation of AB1 (50 mg/L) in 60–120 min, while the work of Zielńska et al. [38,48] using a 180 W mercury lamp in combination with modified TiO_2 catalysts reported degradation of AB1 (50 mg/L) in 20–50 min. Tanaka et al. [39] reported the elimination (mineralization) of 10^{-4} M AB1 in >117 min by Fujititan TP-2 (anatase) illuminated with UV light. Although most works used different amounts of photocatalyst, light intensity, and reactor geometry, most of them rely on photo oxidation and photocatalysis. Sun et al. [49], on the other hand, used Fenton reagents (3 mg/L $\text{Fe}^{2+/3+}$) in combination with sonication for the degradation of AB1 (50 mg/L) in less than 30 min.

For $\text{Cu}_x\text{O-TiO}_2$ catalysts, the role of copper has been published and discussed in the literature in disconnected works attempting the catalytic and photocatalytic degradation of different pollutants. Through the systematic study presented here, we want to assess the factors that are relevant to the catalytic and photocatalytic performance of $\text{Cu}_x\text{O-TiO}_2$ in the degradation of large concentrations of AB1 (100 mg/L).

Because homogeneous and heterogeneous Cu catalysts have shown the ability to produce reactive OH radicals [28,29], under

dark dye degradation can proceed through a Fenton like mechanism, which requires the presence of Cu (I):



There is no clear evidence of Cu (I) species in our catalysts, they can be formed by IFCT during illumination, but under dark conditions an intimate interaction with low coordinated Ti^{3+} centers is required [i.e., $\text{Ti}^{3+} + \text{Cu(II)} \rightarrow \text{Ti}^{4+} + \text{Cu(I)}$]. The Cu-precursor dependence observed in most of the properties measured would indicate that formate-precursors are the less likely to promote Ti^{3+} centers. In the presence of bulky organic anions such as formate, titania nucleation and growth is enhanced by the formation of CuO nucleos, which increase with Cu content. For the inorganic anions, interstitial/substitutional incorporation of Cu (II) disrupt TiO_2 growth, resulting in smaller crystallites as Cu concentration increases.

Concerning the photocatalytic route, Cu (I) produced during illumination by IFCT avoids hole recombination and can reduce adsorbed oxygen opening up the peroxide route [5,16,17]. Additionally, formation of Cu (I) ions by the donation of electrons from unstable Ti^{3+} ions to Cu (II) has been suggested to explain the reduction power of CuO/ TiO_2 systems [49]. The clear differences in the optical properties of catalysts synthesized from organic and inorganic precursors suggest the formation of bulk CuO (i.e., absence of Ti–O–Cu linkages) when formate is used as the Cu-precursor, in detriment to the photocatalytic efficiency in the degradation of AB1. Similar results were found in the degradation of methylene blue with coupled CuO– TiO_2 nanocomposites, where at high loading the bulk form of CuO acts as recombination center [51].

In general, the textural properties show a weak correlation with the catalytic/photocatalytic performance, although it was notorious that catalysts with wide pore-size distribution, or distributions shifted far away from 7 to 9 nm, had lower catalytic/photocatalytic performance. That suggests 7–9 nm as the optimum mesoporosity for $\text{Cu}_x\text{O-TiO}_2$ calcined xerogels in aqueous dye degradation applications. Impregnation techniques show a better correlation between catalytic performance and the textural properties of the titania matrix because Cu ions deposit on the already formed titania surface.

5. Conclusion

We report the synthesis, characterization, and application of mesoporous $\text{Cu}_x\text{O-TiO}_2$ in the catalytic and photocatalytic degradation of AB1. XRD, TEM, and N_2 -adsorption studies confirmed the dependency of crystallite size and textural properties on Cu-precursor and Cu/Ti ratio, particularly at the highest Cu content, with clear differences between the organic and inorganic precursors. Cu (II) was confirmed by XRD, TEM and reflectance measurements, while evidence of Cu (I) was only obtained from the last. At all Cu/Ti ratios, and with all Cu-precursors, the obtained catalysts were mesoporous, underwent pore enlargement as the Cu/Ti ratio increases, and show first order kinetics in AB1 discoloration. Formate-precursor showed the slowest decay curve and this difference magnifies at lower Cu/Ti ratios and under illumination. Differences in titania crystallite size, granule size, surface area, pore distribution, do not seem as relevant as the Cu-content. AB1 degradation under dark conditions proceeds through a Fenton like mechanism, while under illumination it benefits from interfacial charge transfer from TiO_2 to Cu (II). Both mechanisms require an intimate contact between Cu (II) and titania, which is favored in catalysts formed from inorganic Cu-precursors, in contrast to formate precursors that favored bulk CuO, or p-CuO/n- TiO_2 junction acting as recombination center due to the improper position of the semiconductor bands.

Table 3
Amount of AB1 mineralization after 24 min degradation with 0.5 g/L Cu-doped catalysts.^a

Cu salt	Color (Pt–Co)	TOC (mg/L)
– ^b	>550	21.4
$\text{Cu}(\text{HCO}_2)_2$	82	9
$\text{Cu}(\text{NO}_3)_2$	12	7
CuCl_2	3	6

^a Cu/Ti ratio = 0.08, pH = 3, $[\text{H}_2\text{O}_2] = 1.7\text{ mg/L}$, $T = 80^\circ\text{C}$, [AB1] = 100 mg/L.

^b Cu-free calcined xerogels and P25-Degussa.

Acknowledgements

Financial support from DGAPA-UNAM (IN104309), PUNTA-UNAM, CONACYT-México (49100), are gratefully acknowledged, as well as the fellowship (SLA) provided by CONACYT-México. We thank L. Rendón, C. Angeles-Chávez, R. Morán, and M.L. Ramón, for technical assistance and analyses.

References

- [1] T. Horikawa, M. Katoh, T. Tomida, *Micropor. Mesopor. Mater.* 110 (2008) 397–404.
- [2] A.-C. Lee, R.-H. Lin, C.-Y. Yang, M.-H. Lin, W.-Y. Wang, *Mater. Chem. Phys.* 109 (2008) 275–280.
- [3] D.S. Kim, S.J. Han, S.-Y. Kwak, *J. Colloid Interface Sci.* 316 (2007) 85–91.
- [4] I. Paramasivam, J.M. Macak, P. Schmuki, *Electrochem. Commun.* 10 (2008) 71–75.
- [5] H.B. Li, X.C. Duan, G.C. Liu, L.L. Li, *Mater. Res. Bull.* 43 (2008) 1971–1981.
- [6] J.-L. Cao, G.-S. Shao, T.-Y. Ma, Y. Wang, T.-Z. Ren, S.-H. Wu, Z.-Y. Yuan, *J. Mater. Sci.* 44 (2009) 6717–6726.
- [7] K.S. Yoo, T.G. Lee, J. Kim, *Micropor. Mesopor. Mater.* 84 (2005) 211–217.
- [8] X.S. Li, G.E. Fryxell, C. Wang, M.H. Engelhard, *Micropor. Mesopor. Mater.* 111 (2008) 639–642.
- [9] E.L. Crepaldi, G.J.A. Soler-Illia, D. Grosso, F. Cagnol, F. Ribot, C. Sanchez, *J. Am. Chem. Soc.* 125 (2003) 9770–9786.
- [10] J. Konishi, K. Fujita, K. Nakanishi, S. Nishitsuji, M. Takenaka, K. Miura, K. Hirao, *J. Sol-Gel Sci. Technol.* 46 (2008) 63–69.
- [11] M. Andersson, H. Birkedal, N.R. Franklin, T. Ostomel, S. Boettcher, A.E.C. Palmqvist, G.D. Stucky, *Chem. Mater.* 17 (2005) 1409–1415.
- [12] W. Choi, A. Termin, M.R. Hoffmann, *J. Phys. Chem.* 84 (1994) 13669–13679.
- [13] F. Han, V.S.R. Kambala, M. Srinivasan, D. Rajarathnam, R. Naidu, *Appl. Catal. A* 359 (2009) 25–40.
- [14] I.K. Konstantinou, T.A. Albanis, *Appl. Catal. B* 49 (2004) 1–14.
- [15] P. Bouras, E. Stathatos, P. Lianos, *Appl. Catal. B* 73 (2007) 51–59.
- [16] H. Irie, K. Kamiya, T. Shibamura, S. Miura, D.A. Tryk, T. Yokoyama, K. Hashimoto, *J. Phys. Chem. C* 113 (2009) 10761–10766.
- [17] R. López, R. Gómez, M.E. Llanos, *Catal. Today* 148 (2009) 103–108.
- [18] J. Zhang, H. Zhu, S. Zheng, F. Pan, T. Wang, *ACS Appl. Mater. Interfaces* 1 (2009) 2111–2114.
- [19] B. Zhu, X. Zhang, S. Wang, S. Zhang, S. Wu, W. Huang, *Micropor. Mesopor. Mater.* 102 (2007) 333–336.
- [20] K.-H. Kim, S.-K. Ihm, *J. Hazard. Mater.* 146 (2007) 610–616.
- [21] J.-N. Nian, S.-A. Chen, C.-C. Tsai, H. Teng, *J. Phys. Chem. B* 110 (2006) 25817–25824.
- [22] H. Zhu, Y. Wu, X. Zhao, H. Wan, L. Yang, J. Hong, Q. Yu, L. Dong, Y. Chen, C. Jian, J. Wei, P. Xu, *J. Mol. Catal. A: Chem.* 243 (2006) 24–30.
- [23] S. Bennici, P. Carniti, A. Gervasini, *Catal. Lett.* 98 (4) (2004).
- [24] M. Morán-Pineda, S. Castillo, M. Asomoza, R. Gómez, *React. Kinet. Catal. Lett.* 76 (2002) 75–81.
- [25] H.W. Slamet, E. Nasution, S. Purnama, J. Kosela, Gunlazuardi, *Catal. Commun.* 6 (2005) 313–319.
- [26] I.-H. Tseng, J.C.-S. Wu, *Catal. Today* 97 (2004) 113–119.
- [27] A.S. Kovalenko, S.Y. Kuchmii, T.F. Makovskaya, A.V. Korzhak, V.V. Tsyryna, V.I. Yats'kiv, V.G. Il'in, *Theor. Exp. Chem.* 39 (2003) 119–125.
- [28] J.K. Kim, I.S. Metcalfe, *Chemosphere* 69 (2007) 689–696.
- [29] D. Mantzavinos, *Water, Air, Soil Pollut.* 3 (2003) 211–221.
- [30] N. Wang, J. Li, L. Zhu, Y. Dong, H. Tang, *J. Photochem. Photobiol. A* 198 (2008) 282–287.
- [31] R.S.K. Wong, J. Feng, X. Hu, P.L. Yue, *J. Environ. Sci. Health Part A* 39 (2004) 2583–2595.
- [32] K. Chiang, R. Amal, T. Tran, *Adv. Environ. Res.* 6 (2002) 471–485.
- [33] J. Xiaoyuan, D. Guanghui, L. Liping, C. Yingxu, Z. Xiaoming, *J. Mol. Catal. A: Chem.* 218 (2004) 187–195.
- [34] J.C.S. Wu, I.-H. Tseng, W.-C. Chang, *J. Nanopart. Res.* 3 (2001) 113–118.
- [35] D. Nazimek, W. Ciwikla-Bundyra, *Catalysis Today* 90 (2004) 39–42.
- [36] A. Yin, X. Guo, K. Fan, W.-L. Dai, *Appl. Catal. A* 377 (2010) 128–133.
- [37] F. Wang, G. Lu, *Int. J. Hydrogen Energy* (2010), doi:10.1016/j.ijhydene.2009.12.186.
- [38] J. Grzechulska, A.W. Morawski, *Appl. Catal. B: Environ.* 36 (2002) 45–51.
- [39] K. Tanaka, K. Padernpole, T. Hisanaga, *Wat. Res.* 34 (2000) 327–333.
- [40] X. Bokhimi, A. Morales, O. Novaro, T. López, O. Chimal, M. Asomoza, R. Gómez, *Chem. Mater.* 9 (1997) 2616–2620.
- [41] O.V. Komova, A.V. Simakov, V.A. Rogov, D.I. Kochubei, G.V. Odegova, V.V. Kriventsov, E.A. Paukshtis, V.A. Ushakov, N.N. Sazonova, T.A. Nikoro, *J. Mol. Catal. A: Chem.* 161 (2000) 191–204.
- [42] J. Chen, M. Yao, X. Wang, *J. Nanopart. Res.* 10 (2008) 163–171.
- [43] E. Vigil, F.A. Fernández-Lima, J.A. Ayllón, E. Pedrero, I. Zumeta, B. González, L. Curbelo, H.D. Fonseca Filho, M.E.H. Maia da Costa, C. Domingo, M. Behar, F.C. Zawislak, *Micropor. Mesopor. Mater.* 109 (2007) 560–566.
- [44] <http://www.epa.gov/safewater/contaminant>.
- [45] H.-Y. Shu, M.-C. Chang, *Dyes Pigments* 70 (2006) 31–37.
- [46] H.-Y. Shu, M.-C. Chang, H.-J. Fan, *J. Hazard. Mater.* B113 (2004) 201–208.
- [47] A.C.-K. Yip, F.L.-Y. Lam, X. Hu, *Chem. Eng. Sci.* 62 (2007) 5150–5153.
- [48] B. Zielińska, J. Grzechulska, A.W. Morawski, *J. Photochem. Photobiol. A* 157 (2003) 65–70.
- [49] J.-H. Sun, S.-P. Sun, J.-Y. Sun, R.-X. Sun, L.-P. Qiao, H.-Q. Guo, M.-H. Fan, *Ultrason. Sonochem.* 14 (2007) 761–766.
- [50] B. Xu, L. Dong, Y. Chen, *J. Chem. Soc., Faraday Trans.* 94 (1998) 1905–1909.
- [51] G. Li, N.M. Dimitrijevic, L. Chen, T. Rajh, K.A. Gray, *J. Phys. Chem. C* 112 (2008) 19040–19044.